Alzheimer's
Research & Therapy

RESEARCH

Open Access

# Digital twins and non-invasive recordings enable early diagnosis of Alzheimer's disease

Lorenzo Gaetano Amato[1,2], Michael Lassi[1,2], Alberto Arturo Vergani[1,2], Jacopo Carpaneto[1,2], Salvatore Mazzeo[3,4,5], Valentina Moschini[6], Rachele Burali[7], Giovanni Salvestrini[8], Carlo Fabbiani[7], Giulia Giacomucci[9], Giulia Galdo[9], Carmen Morinelli[9], Filippo Emiliani[9], Maenia Scarpino[9], Sonia Padiglioni[9], Benedetta Nacmias[7,9], Sandro Sorbi[7,9], Antonello Grippo[8], Valentina Bessi[9] and Alberto Mazzoni[1,2*]

## Abstract

**Background** The diagnosis of Alzheimer's disease (AD) in its preclinical stages, such as subjective cognitive decline (SCD), is crucial for a timely management of the condition. However, current early diagnostic methods are unsuitable for preclinical screenings due to limited availability and diagnostic reliability. Additionally, reliance on invasive and scarcely available methods exacerbates the underdiagnosis of AD in its preclinical forms.

**Methods** We introduce an early diagnostic pipeline based on the Digital Alzheimer's Disease Diagnosis (DADD) digital twin model, which derives personalized AD biomarkers from non-invasive electroencephalographic (EEG) recordings. These biomarkers reconstruct patient-specific neurodegeneration, capturing synaptic and connectivity degeneration mechanisms. Digital biomarkers were used to predict cerebrospinal fluid (CSF) biomarker positivity for AD and clinical conversions at follow-up in 124 participants with varying degrees of cognitive decline, including a control group of 19 healthy subjects.

**Results** Digital biomarkers derived from the DADD model: i) Robustly distinguished SCD from healthy participants, improving classification accuracy by 7% compared to standard EEG biomarkers; ii) Identified patients positive for CSF biomarkers of AD with 88% accuracy (significantly outperforming standard EEG biomarkers, which achieved 58% accuracy); iii) Predicted follow-up conversions to clinical cognitive decline with 87% accuracy (compared to 54% accuracy for standard EEG biomarkers).

**Conclusions** The DADD model provided robust digital AD biomarkers with strong diagnostic and prognostic value for preclinical AD, enabling the prediction of CSF biomarkers and clinical conversions using only non-invasive EEG recordings. This is particularly important as preclinical patients, such as those with SCD, are often excluded from diagnostic procedures like lumbar puncture. Predicting CSF biomarkers by combining digital twins with non-invasive recordings could revolutionize AD diagnosis in its early stages, paving the way for the clinical application of digital twins in AD diagnostics.

**Trial registration** Clinical Trial identifier: NCT05569083 (submitted 2022–08-24).

**Keywords** Subjective Cognitive Decline, Biomarkers, Diagnosis, Prognosis

*Correspondence:
Alberto Mazzoni
alberto.mazzoni@santannapisa.it
Full list of author information is available at the end of the article

## Background

Management of Alzheimer's disease (AD) is emerging as one of the key medical challenges of our time. According to current projections, the total number of people living with dementia worldwide is expected to reach 140 million by 2050 [1, 2], with the associated costs soaring to an astronomical $17 trillion [3]. As no viable therapeutic strategy is currently available, early diagnosis becomes a crucial requirement for a timely management of the disease [4].

One of the earliest indicators of AD is a condition known as subjective cognitive decline (SCD) [5]. SCD refers to the experience of persistent memory problems or cognitive difficulties that are noticeable to the individual but not yet detectable by standardized cognitive tests [5]. There is strong evidence that this condition may reflect structural neurodegeneration mechanisms associated with AD [6, 7], preceding overt symptoms by years or decades [7, 8]. However, the majority of SCD patients will remain stable for their entire lifetime, challenging the characterization of this condition as an early AD phase [9]. Therefore, recognizing and addressing SCD is critical for early intervention [10].

It is estimated [11, 12] that an early diagnosis in the SCD phase, enabling timely drug therapy to slow disease progression and reduce hospitalizations, could decrease the number of AD patients by about a third (36%) and overall costs by roughly a fifth. Furthermore, the early phases of the disease are those in which cognitive training approaches are most fruitful [13]. However, the majority of AD cases remain undiagnosed, with percentages ranging from 50 to 80% in developed countries, reaching 90% in developing countries [1]. The imperative, therefore, is to develop more accessible, cost-effective, and non-invasive diagnostic tools that can be used for early detection during preclinical phases such as SCD [4].

Electroencephalography (EEG) has emerged as a widely adopted tool for analyzing neural processes in both healthy and pathological conditions [14]. EEG has been extensively used to investigate the effects of AD and cognitive decline in the electrical brain activity [15–17] measured during cognitive tasks [17] or in the resting state [16]. The principal positive aspects of EEG are the reduced costs and wide availability, contrasting with more expensive diagnostic methods such as MRI and PET scans [18]. However, EEG exhibits some notable limitations, particularly regarding spatial resolution [19] and volume conduction effects [20]. Moreover, most studies focusing on EEG-based diagnosis and classification of cognitive decline and dementia often employ deep-learning techniques [21–25], which have gained widespread popularity in the past years. While these techniques may achieve high performance in classifying pathological states [22, 23], they are hard to translate into clinical settings [26, 27] due to their lack of interpretability, and their demand for large datasets. Particularly, no diagnostic pipeline for AD based on EEG recordings has reached clinical use.

Computational models and digital twins represent a promising solution to address the gap between EEG high temporal resolution and the need for investigating structural neurodegeneration mechanisms at a finer scale [28]. These models allow to simulate the effects of multiscale structural alterations on brain activity [29], inferring causal and interpretable relationships between modeled alterations and their impact on simulated signals [30–34]. However, these models are scarcely used in clinical settings, as they are rarely implemented with the translational aim of deriving novel biomarkers to characterize patient's clinical state.

In this study, we present the DADD (Digital Alzheimer's Disease Diagnosis) model, which provides digital biomarkers of Alzheimer's disease leveraging personalized brain modeling and EEG recordings (Fig. 1A). The DADD model was tested, in a previous iteration, to capture alterations in resting-state EEG within the AD continuum [35] and to bridge between neurodegeneration and neural activity alterations alongside cognitive decline evolution using task EEG data [36]. By incorporating well-documented disease mechanisms associated with AD [6, 29, 37–39], DADD reconstructs a personalized digital twin for each patient, reconstructing individual levels of neurodegeneration from EEG recordings collected during task execution. The DADD model demonstrated high accuracy in predicting both cerebrospinal fluid (CSF) biomarkers of AD and conversions to clinical cognitive decline (Fig. 1B), paving the way for the use of personalized brain models in clinical practice.

## Methods

### Participants recruitment

Participants were recruited as part of the PREVIEW project [40], a longitudinal study on preclinical forms of AD such as the SCD condition (Clinical Trial identifier: NCT05569083, first submitted on 24/08/2022). A total of 126 self-referring patients with cognitive complaints participated in the study, of whom 86 were determined to be SCD (age: 67.04 ± 9.54 years). The other 40 were classified as mild cognitive impairment patients (MCI) and were excluded from the analysis, except for the 19 MCI patients with available CSF data, included only in the pipeline for the prediction of CSF positivity (see the *Cerebrospinal fluid analysis* paragraph). We also included a control group of 19 healthy subjects (CTR, age: 64.06 ± 4.93) that volunteered for the study. Classification into diagnostic groups was based on extensive genetic and

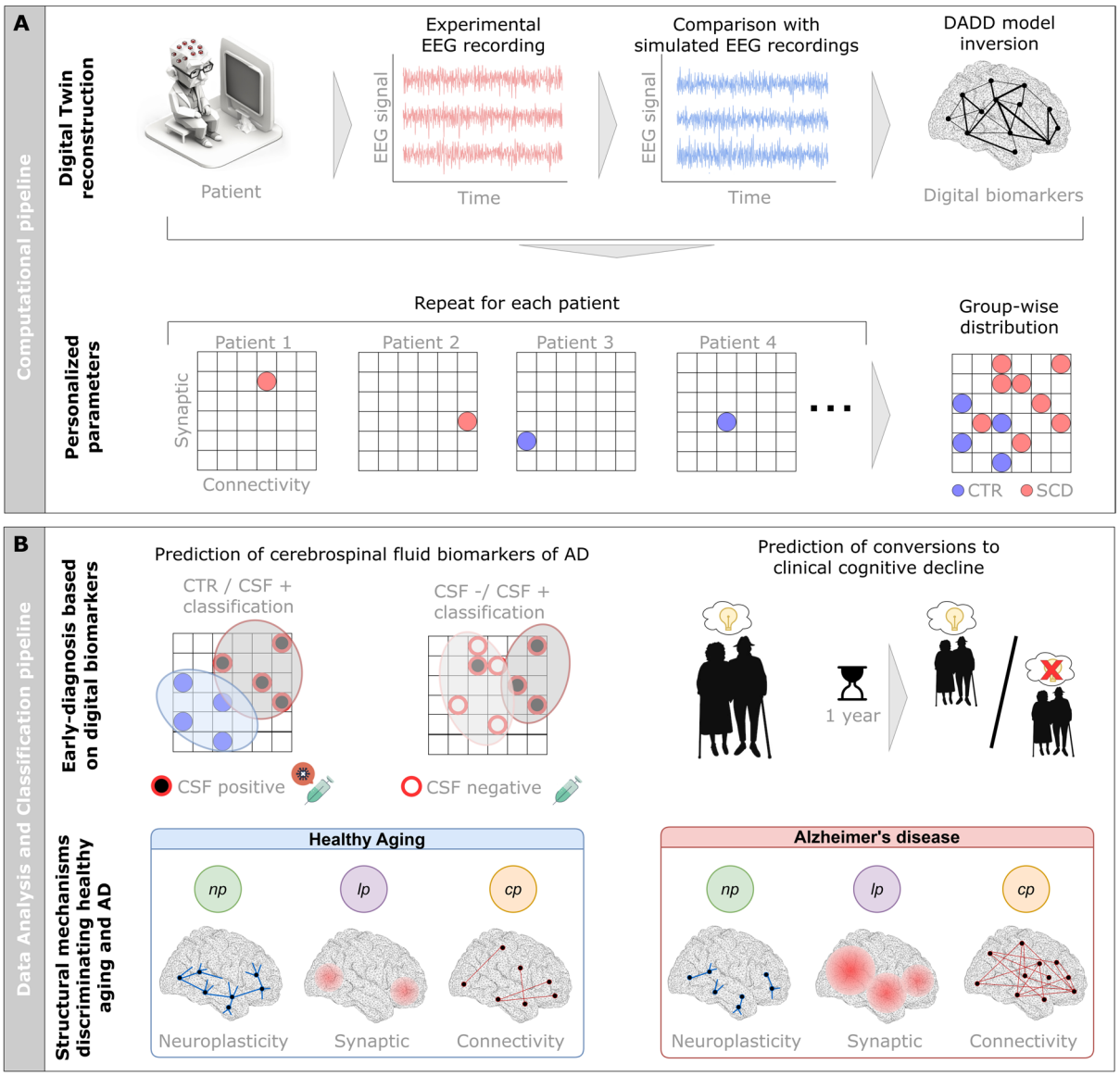


**Fig. 1** The DADD model: providing digital biomarkers to support early diagnosis of Alzheimer's disease. **A**: EEG signals were collected from healthy subjects and SCD patients during task execution. Personalized digital biomarkers reflecting individual neurodegeneration levels were reconstructed through model inversion by maximizing the similarity between experimental and simulated signals. The procedure was repeated for all patients, enabling the analysis of digital biomarkers at a group-wise level. **B**: Digital biomarkers were employed to classify patients positive for CSF markers of AD-type dementia (CSF +). Digital biomarkers supported both a classification between CSF + patients and CTR subjects, and between CSF + patients and patients negative to CSF markers of AD (CSF-). The same biomarkers also predicted patients converted toward the clinical condition of mild cognitive impairment. The performance of DADD-based classifications was compared with the performance obtained using standard EEG biomarkers as classifying features. The analysis of digital biomarkers allowed the identification of structural mechanisms discriminating between healthy aging and Alzheimer's disease

behavioral tests, following the NIA-AA criteria for subjective cognitive decline and mild cognitive impairment diagnosis [41]. Guidelines for participants recruitment (including inclusion/exclusion criteria), cognitive task architecture and cognitive evaluation are discussed in Supplementary Methods.

### EEG recordings

EEG data were collected from participants who met the inclusion criteria outlined in the study. The EEG recordings were conducted while participants were seated in a comfortable position during the execution of the cognitive task. Signals were collected using the 64-channels Galileo-NT system (E.B. Neuro S.p.a.), with sensor

topography following the extended 10/20 system. Unipolar signals were recorded at a sampling rate of 512 Hz, and electrode impedances, monitored throughout EEG acquisition, were maintained in the 7–10 kOhm range. Portions of the signal where impedance deviated outside of the 7–10 kOhm range were discarded.

#### Experimental EEG pre-processing and ERP extraction

The EEG pre-processing pipeline was implemented using MATLAB with the commercially available EEGLAB Toolbox [42]. Pre-processing followed the steps delineated by the PREP pipeline [43], including: (i) band-pass filtering in the 1—45 Hz range using a Butterworth filter, (ii) identification and subsequent removal of noisy channels, (iii) average re-referencing, (iv) Independent Component Analysis (ICA)-based detection and elimination of artefactual components. Please note that the last step was custom-built and is not included in the PREP pipeline.

The cognitive task required the participant to recognize the correct shape (an upward triangle ▲) among two confounding shapes (a downward triangle ▼ and a diamond ◊). Each trial of the task experiment lasted 1000 ms, divided into two parts: stimulus presentation in the first 200 ms, and participant response in the subsequent 800 ms.

EEG signals were analyzed to extract Even Related Potentials (ERPs). ERPs were epoched in the [0, 750] ms window, aligning the 0 ms instant with stimulus presentation. We analyzed the timeframe of encoding processing (Supplementary Fig. 1A), which includes the P1 and N1 neural markers [15] (respectively, the first positive and negative deflection after stimulus onset, with the P1 usually centered in the [50, 100] ms window and the N1 usually centered in the [100, 150] ms window, see Supplementary Fig. 1B). Both the P1 and the N1 components are recorded from occipital channels (PO7, PO8, O1, O2, Oz). P1 and N1 ERP amplitudes were determined by computing integrals in their respective timeframe. To investigate decision processing (Supplementary Fig. 1C), we also analyzed the [300 ms, 500 ms] window in central channels (FC1, FCz, FC2, C1, Cz, C2), associated with the P2 component [15], the second positive deflection after stimulus onset (see Supplementary Fig. 1D). While this positive deflection usually occurs at around 300 ms after stimulus presentation, we anticipated the P2 to peak at around 400 ms, due to age effects. Similarly to P1 and N1, P2 ERP amplitudes were determined by computing the integral in its timeframe. We also analyzed the P1 and N1 peak amplitudes and latencies (timings of peak values with respect to stimulus onset), which presented no significant differences across groups.

Extra-occipital Functional connectivity (FC) was computed as the percentage of channels beyond the occipital cluster showing high positive correlations ($r > 0.75$) with occipital channels during the encoding timeframe. In the main text it is abbreviated as FC for the sake of brevity. A value close to 0% indicated no significant correlations, while a value near 100% suggested strong correlations across the scalp. Only significant correlations (Bonferroni-Holm $p < 0.05$) were considered using Spearman's non-parametric measure. For simulated EEG signals, ERPs extraction and FC computation followed the same methodology.

The DADD model has been already applied to capture the evolution of resting state EEG activity alongside the AD continuum [35]. Analyzing resting-state EEG, different metrics emerged as the most informative about patient's condition, namely global functional connectivity and relative power spectral density. However, in previous studies from our group we analyzed task EEG data using both standard statistical methods [44] and by using the DADD model [36], finding that these metrics presented low discrimination power about patient's condition in task EEG. These studies also highlighted that ERP features such as the N1 component and extra-occipital functional connectivity were the most informative task-condition EEG metrics, ultimately leading to our choice of using these metrics for the determination of digital biomarkers.

#### Cerebrospinal fluid extraction

We included in the study 25 SCD patients and 19 MCI patients that volunteered for cerebrospinal fluid extraction via lumbar puncture. Samples were analyzed for Alzheimer's biomarkers such as Abeta42, ratio of Abeta42/Abeta40, t-tau and p-tau. Cut-off value for the determination of positivity were adopted from Fujirebio guidelines [45]. CSF analysis is discussed in detail in Supplementary Methods.

#### Follow-up data and converted patients

As part of the longitudinal study, enrolled SCD patients were re-examined after 1 year to assess their clinical condition. The same diagnostic battery of tests was performed again on the patients to assess their cognitive state. The EEG examination was not repeated, as it was not included in the initial study design. Follow-up tests are ongoing, as of today, 27 SCD patients have been re-examined and included in this study, 7 of which transitioned to the clinical condition of mild cognitive impairment [41]. No MCI patient transitioned to full AD during the study.

### DADD model and simulated signal

The DADD Model is discussed in detail in previous publications from our group [35, 36]. Briefly, it represents the brain cortex as a network of 76 interacting regions using The Virtual Brain platform (TVB) [46]. Neural activity was modeled using a modified Jansen-Rit neural mass model [47], and structural connectivity was derived from the TVB database. EEG signals were simulated by projecting local activity onto a virtual electrode grid situated on a 3D scalp model. The projection comprises the computation of electrical field transmission across layers of difference conductance, mimicking brain, skull and scalp tissues.

Simulated neurodegeneration is regulated by parameters cp and lp, governing connectivity and synaptic degeneration, respectively. Increasing either parameter leads to a more severe level of structural neurodegeneration. A third parameter, called np, describes connectivity rewiring effects. Biophysically, lp reflects cortical hypo-inhibition and hyperexcitation [39], while cp portrays white matter atrophy [6] and the np parameter describes the neuroplastic effects on connective rewiring [38, 48].

In our model, each node represents a brain region connected by a high-fidelity structural connectivity matrix [49]. Synaptic degeneration is governed by the lp parameter with the equation:

$$\begin{aligned} \tau_i &\rightarrow \tau_i^{HC} + lp \times \left(\tau_i^{\max} - \tau_i^{HC}\right) \\ \tau_e &\rightarrow \tau_e^{HC} + lp \times \left(\tau_e^{\min} - \tau_e^{HC}\right) \end{aligned}, 0 < lp < 1 \qquad (1)$$

Connectivity alterations are described by both the connectivity degeneration parameter cp and by the neuroplastic rewiring parameter np, according to the equation:

$$C_{\text{weight}} \rightarrow \begin{cases} C_{\text{weight}}^{HC} - cp \times C_{\text{weight}}^{max}, & \text{if } C_{\text{length}} > C_{\text{length}}^{\text{th}} \\ C_{\text{weight}}^{HC} + np \times cp \times C_{\text{weight}}^{\max}, & \text{if } C_{\text{length}} < C_{\text{length}}^{th} \end{cases}, 0 < cp < 1 \qquad (2)$$

The lp parameter affects local neural dynamics, while both cp and np influence the structural connectivity matrix. Particularly, the second equation decreases long range connections in affected nodes depending on cp values, while it increases short range connections by an amount determined by the $np \times cp$ product. Affected nodes followed the conventional early Braak staging for amyloid deposition [50], and can be consulted in our previous work [36]. The $C_{\text{length}}^{th}$ threshold value was chosen as one third of the maximum length value $C_{\text{length}}^{\max}$ [35]. Both lp and cp parameters range from 0 to 1, with 1 indicating the most severe condition. The np parameter is instead comprised between 0 and 2.5, with the highest value indicating strong neuroplastic rewiring in the brain network. In the main text, np values are normalized between 0 and 1 to facilitate comparisons with other parameters.

The values in Eqs. 1 and 2 were derived from biophysical constraints, and can be consulted from our previous work [36].

To further investigate the role played by structural alterations in influencing cognitive performance, we computed additional metrics, called Total Degeneration and Connective Loss.

Total Degeneration is the squared sum of the connectivity and synaptic degeneration of the network, according to the equation:

$$TotalDegeneration = \sqrt{cp^2 + lp^2} \qquad (3)$$

The Connective Loss metrics represents instead the ratio between connectivity degeneration parameter and neuroplastic rewiring parameter, corresponding to the ratio between average decrease in connections and rewiring in the DADD model. The equation for Connective Loss is:

$$ConnectiveLoss = \frac{cp + 1}{np + 1} \qquad (4)$$

Additive +1 values were inserted to ensure that the Connective Loss parameter was defined even for np =0. The three additional digital biomarkers reported in Eqs. 3– 5 were then normalized between 0 and 1 to facilitate comparisons.

Digital biomarkers were obtained from patient-specific EEG recordings by a model inversion pipeline that compared experimental recordings with signals simulated using the DADD model. The model inversion pipeline is discussed in detail in Supplementary Methods.

### Machine learning pipeline

We implemented a machine learning pipeline to classify CTR and SCD patients using features derived from cognitive and electrophysiological measures. The process began with feature selection from the ERP dataset, using mutual information, where we identified the most informative biomarkers among standard EEG ones (N1 integral, FC, Reaction Time, Accuracy) and digital ones (model parameters).

We then performed classifications between CTR subjects and SCD patients, as well as identification of CSF + patients (CSF +/CTR classification) and prediction of positivity to CSF in cognitive decline patients (CSF +/CSF- classification) testing several machine learning models. We also performed a classification between SCD patients who remained stable and SCD patients who converted during the follow-up. All classifications were aimed at deriving interpretable decision boundaries for prediction of CSF positivity and clinical conversions. Since both the determination of decision boundaries and the subsequent classifications were operated in the same dataset, we adopted a nested cross-validation approach to reduce overfitting.

Machine learning pipelines for all classifications are described in detail in Supplementary Methods.

#### Statistical Analysis and outlier management

Comparisons across groups were conducted using the Mann–Whitney U test. Outliers were defined as datapoints that ranged more than 3 $\sigma$ from the nearest datapoint, where $\sigma$ is the standard deviation of the sample. Only one outlier was identified in the Connective Loss of the CTR group, that is thus reduced to $n = 18$ subjects. The inclusion or exclusion of the outlier did not alter the significance of the Mann–Whitney test used to determine the group differences of the Connective Loss biomarker.

McNemar's test was employed to investigate statistical differences between classifications.

For all tests, the statistical significance threshold was put at $p = 0.05$, with the additional requirement of presenting a large size effect, measured with Cohen's d. (the adopted threshold for large size effect was Cohen's $d > 0.5$).

All simulations, data analysis and machine learning pipelines were implemented in Python 3.10, with simulations conducted using The Virtual Brain software, and analyzed with standard Python packages such as SciPy, NumPy, and Pandas. KDE plots were realized with the kdeplot function of Seaborn Python library. The classifications were performed using the Scikit-Learn package.

## Results

#### The DADD model provides digital biomarkers that robustly discriminate between SCD and healthy controls

We reconstructed personalized digital twins using EEG recordings collected during cognitive task execution from 86 subjective cognitive decline (SCD) patients and 19 age-matched ($U = 990.5$, $p = 0.15$ for age differences between groups) healthy subjects. Relevant demographic information about participants can be consulted in Supplementary Table 1. Statistical analysis revealed no significant group differences in cognitive task performance, as measured by task accuracy, reaction time and F-measure [14] (Supplementary Table 2). EEG recordings were analyzed to extract event-related potentials (ERPs) elicited by task execution. We analyzed standard ERP components, specifically the P1, N1 and P2 components [15] (Supplementary Fig. 1) as well as extra-occipital functional connectivity (FC, see Methods) to assess the spatial extent of neural activity during task execution [51].

Statistical analysis revealed no significant differences between groups in the P1 and P2 components (non-significant differences for P2: $U = 800.0$, $p = 0.16$, and mildly significant differences with small effect size for P1: $U = 51.0$, $p = 0.036$, $d = -0.3$). The N1 component presented significant group differences ($U = 1183$, $p = 0.006$, $d = 1.0$, Supplementary Fig. 2A). FC presented a trend toward significant differences ($U = 1078$, $p = 0.058$, Supplementary Fig. 2B).

We employed the DADD model to reconstruct personalized parameters from individual EEG recordings [35] (see Methods and Fig. 2A). DADD parameters captured Alzheimer's-related micro- and macroscopic structural neurodegeneration mechanisms (see Methods). These mechanisms included synaptic micro-scale degeneration (lp parameter) and large-scale connectivity disruptions (cp parameter), also considering neuroplastic connectivity rewiring (np parameter). After estimating each patient's individual parameters, we analyzed their group-wise distributions to assess their role as digital AD biomarkers (Fig. 2B).

Digital biomarkers presented profound differences between groups. When compared with SCD patients, CTR subjects showed different levels of connectivity and synaptic degeneration (particularly presenting lower cp levels), and higher levels of neuroplastic rewiring (Fig. 2C). Statistical analysis (Fig. 2D) confirmed significant differences across groups in connectivity degeneration ($U = 1078.5$, $p = 0.029$, $d = -0.6$) while differences in synaptic degeneration were non-statistically significant ($U = 880.0$, $p = 0.60$). Additionally, neuroplastic rewiring levels were significantly higher in CTR subjects ($U = 474.0$, $p = 0.004$, $d = 0.8$).

We conducted a deeper analysis of np values, dividing it into quintiles and investigating group-wise distributions. The analysis revealed that group-wise differences were significant only in the bottom quintile in which SCD patients were predominant (38% of SCD and 11% of CTR, $\chi^2 = 7.43$, $p = 0.012$ with Bonferroni-Holm correction) and in the upper quintile, in which CTR subjects were predominant (12% of SCD and 36% of CTR, $\chi^2 = 5.55$, $p = 0.018$ with Bonferroni-Holm correction, see Fig. 2E).

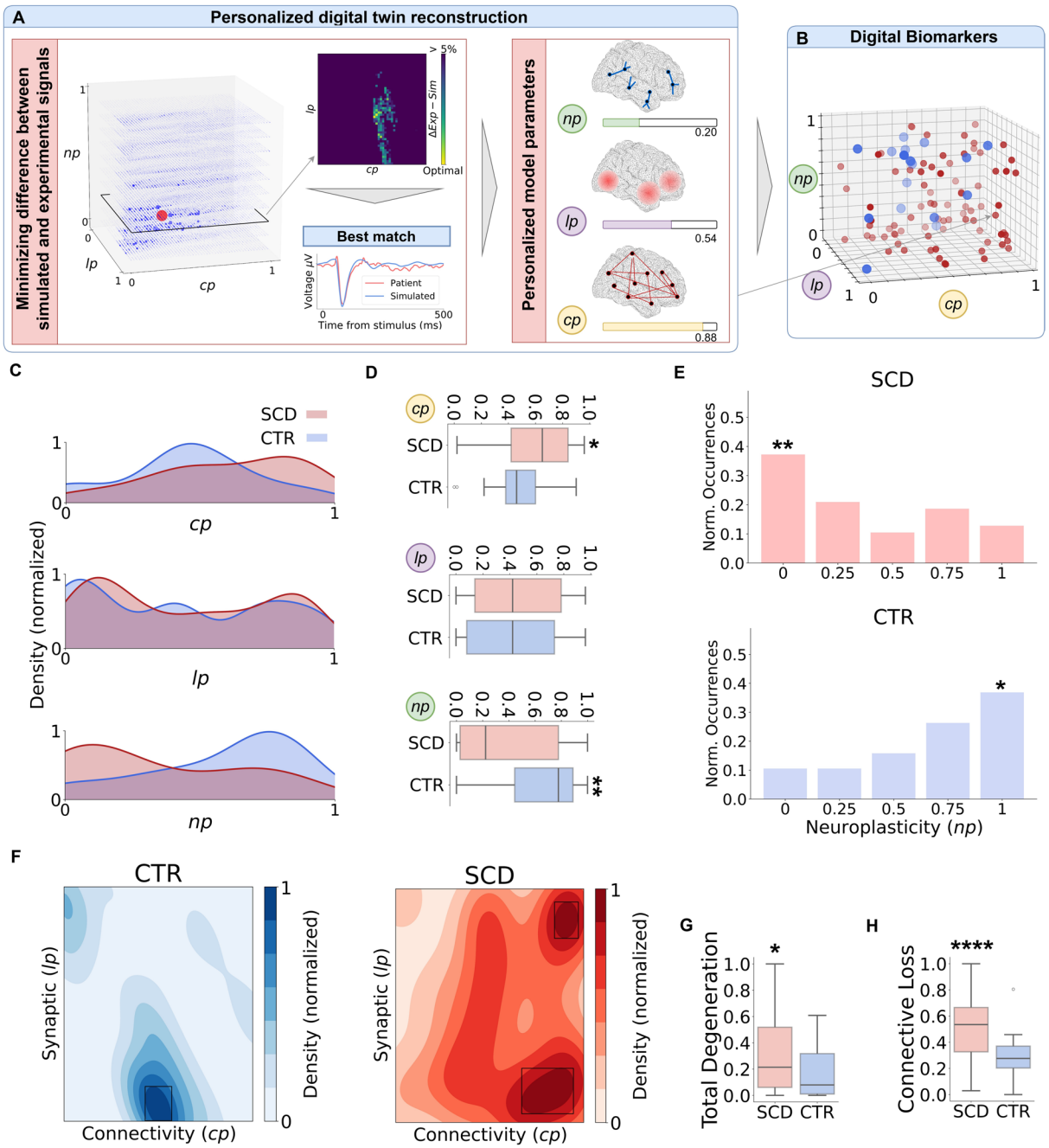


**Fig. 2** Digital biomarkers robustly discriminate between CTR and SCD participants. **A**: Pipeline for the determination of personalized digital twins from experimental recordings: A loss function between simulated and experimental signals is computed for all possible DADD parameter combinations to find optimal values for each patient. **B** Distributions of personalized connectivity degeneration, synaptic degeneration and neuroplastic rewiring parameters (cp, lp, and np, respectively) for the CTR and SCD groups. **C**: Group-wise distributions of individual digital biomarkers (cp on top, lp in the middle and np at the bottom). **D**: Boxplot comparison of digital biomarkers (cp on top, lp in the middle and np at the bottom) between groups. Whiskers represent 1.5 times the interquartile values. **E**: Distribution of neuroplastic rewiring parameters in the CTR (top) and SCD (bottom) groups, divided into quintiles. The significance of group differences in each quintile was determined with a $\chi^2$ test with multiple comparisons correction (see main text). **F**: Distribution of connectivity and synaptic degeneration parameters in the CTR (left) and SCD (right) groups. Peak values were inferred with KDE, with confidence intervals visualized as black rectangles in the plot. The CTR group presented a peak for low values of the lp parameter (see main text) while the SCD group had a peak at low lp and one at higher lp values. **G**: Comparison of Total Degeneration between groups. **H**: Comparison of Connective Loss between groups. Notation is the same as in (C). Significance notation: * stands for $p < 0.05$ after, ** stands for $p < 0.01$, *** stands for $p < 0.001$, *** stands for $p < 0.0001$

Next, we investigated the distribution of model parameters lp and cp (the two parameters capturing neurodegenerative effects) across groups with a kernel density estimation (KDE) routine. Despite synaptic degeneration presenting no statistically significant differences across groups (Fig. 2D), the KDE analysis revealed that SCD patients presented one additional peak with respect to CTR subjects at higher lp values (Fig. 2F, SCD peaks at lp = 0.08 and lp = 0.88, CTR peak at lp = 0.04). Both SCD peaks were at higher cp values than the CTR one (SCD peaks at cp = 0.90 and cp = 0.94, CTR peak at cp = 0.48).

We then used the lp, cp and np parameters to extract additional digital biomarkers. The first additional biomarker was called Total Degeneration, computed as the squared sum of neurodegenerative parameters cp and lp (Eq. 3). Total Degeneration values presented statistically significant differences between groups (Fig. 2G, U = 1085.0, $p$ = 0.026, d = 0.5). The other additional biomarker was called Connective Loss, computed from the connectivity degeneration parameter cp and the neuroplastic rewiring parameter np. Connective Loss reflects the ratio between the loss of long-range connections and the increase in short-range connections (Eq. 4). We analyzed the group-wise differences in this biomarker, computing individual values from the personalized values of cp and np.

Notably, Connective Loss was higher in SCD patients with very high significance (Fig. 2H, U = 1256.0, $p$ = 0.0003, d = −1.0). This holds great importance for the clinical use of computational models in identifying diagnostic groups, as this digital biomarker emerged as the quantity that more robustly discriminated between CTR and SCD participants.

### Digital biomarkers outperform standard biomarkers in classifying SCD patients and healthy participants

We then evaluated the performance of both standard EEG biomarkers (also including cognitive metrics related to task performance) and digital biomarkers in classifying SCD and CTR participants. First, we assessed the information carried by both standard EEG and digital biomarkers on diagnostic groups. This was done with a feature selection routine based on mutual information (MI) computation (Fig. 3A). Digital biomarkers presented higher MI, with Connective Loss and Neuroplasticity being the most informative (respectively mean MI = 0.10 and mean MI = 0.06). The most informative standard features were the N1 integral and FC values (respectively mean MI = 0.08 and mean MI = 0.05). The cumulative information about the diagnostic group was significantly higher for digital biomarkers than for standard EEG biomarkers (considering the top two for each class: 0.16 ± 0.02 vs 0.13 ± 0.01, U = 29,492.0, $p$ < 0.00001, Fig. 3B). Mean values and standard deviation values were determined by Jackknife resampling (see Methods).

Subsequently, we employed a machine-learning pipeline to classify SCD and CTR participants. We tested several algorithms (see Supplementary Methods), eventually choosing a Random Forest model. We used either standard EEG biomarkers or digital biomarkers as diagnostic features, choosing between the ones considered in the feature selection routine.

Digital biomarkers outperformed standard EEG biomarkers in terms of accuracy (79% ± 3%, compared to 72% ± 7% for standard EEG biomarkers). McNemar's test confirmed the significant differences between the two sets of biomarkers in terms of classification performance ($p$ = 0.031). Additionally, we computed the area under the Receiver Operating Characteristic (ROC) curve (AUC) for both classifications. The classification based on digital biomarkers achieved a higher AUC (0.79 ± 0.03) compared to the classification using standard EEG biomarkers (AUC = 0.70 ± 0.03). ROC plots for these comparisons are presented in Fig. 3C, while accuracy is reported in Fig. 3D.

### Digital biomarkers predict cerebrospinal fluid biomarkers of AD and conversions toward clinical cognitive decline

Both standard EEG and digital biomarkers achieved good performances in classifying SCD and CTR participants. We then evaluated the ability of both sets of biomarkers to predict the presence of cerebrospinal fluid biomarkers of Alzheimer's disease in cognitive decline patients. We included 44 patients who underwent CSF extraction: 25 SCD patients and 19 age-matched patients with mild cognitive impairment (MCI). Among these, 16 patients tested positive for amyloid-beta and tau protein (CSF +, see Methods), while 28 were negative (CSF-).

We first analyzed how standard EEG biomarkers and digital biomarkers differed between CTR subjects and CSF + patients (see Methods and Fig. 4A). Among standard biomarkers, only the N1 integral values showed significant differences between CTR and CSF + participants (Supplementary Fig. 3A, U = 83.0, $p$ = 0.023, d = 1.0). Connective Loss was the digital biomarker that most strongly discriminated between groups, presenting statistically relevant differences (Supplementary Fig. 3B, U = 217.0, $p$ = 0.012, d = 1.1).

We then trained a machine-learning model (see Methods) to identify CSF + patients (Fig. 4A) by performing a CSF +/CTR classification using either standard EEG or digital biomarkers. Comparing results obtained with the two sets of biomarkers, we found that digital biomarkers presented higher accuracy (88% ± 4% vs 58% ± 6% for digital biomarkers, confusion matrices in Fig. 4B) and average AUC (0.80

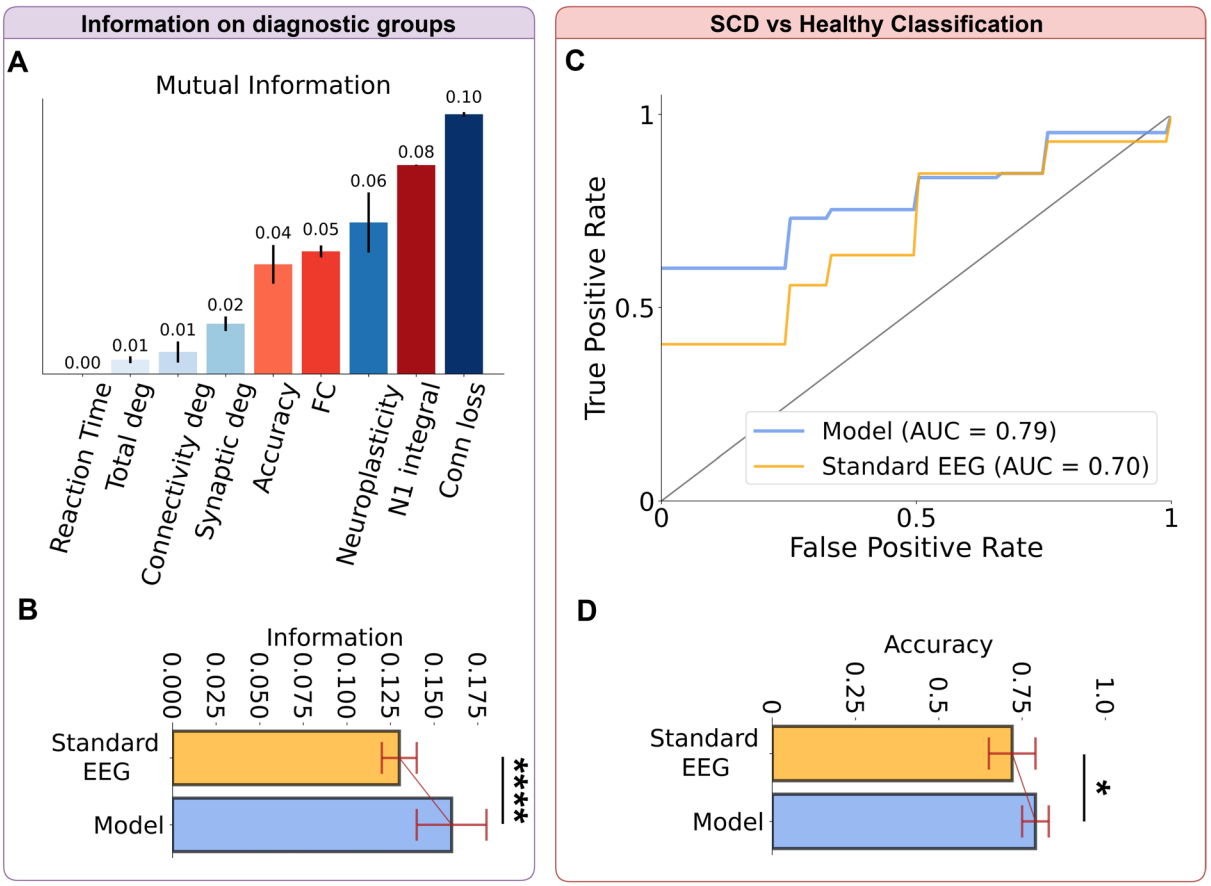


**Fig. 3** Digital biomarkers outperform standard biomarkers in distinguishing SCD patients from healthy participants. **A**: Mutual information values about diagnostic group conveyed by standard EEG (red hue) and digital (blue hue) biomarkers. **B**: Cumulative information about diagnostic groups conveyed by standard and digital biomarkers. **C**: ROC curve for SCD-CTR classification based on standard EEG biomarkers and digital biomarkers. AUC was higher for the DADD-based classification. **D**: Accuracy of SCD-CTR classification based on standard EEG or digital biomarkers. Also accuracy was higher for the DADD-based classification. Significance notation: * stands for $p < 0.05$, **** stands for $p < 0.00001$. Error bars represent standard deviation values. Neuroplasticity represents the np parameter

$\pm 0.02$ vs $0.57 \pm 0.03$ for standard biomarkers, average ROCs in Fig. 4C). Analyzing precision, defined as the ratio between predicted CSF + and actual CSF + patients, standard biomarkers led to inconclusive results, obtaining an average of 8/16 CSF + patients correctly identified (50% ± 7% precision, Fig. 4D), while digital biomarkers achieved an average of 14/16 CSF + patients correctly identified (87% ± 4% precision). A McNemar's test confirmed the significant difference between DADD-based and standard EEG classifications ($p = 0.002$).

(See figure on next page.)

**Fig. 4** Digital biomarkers predict cerebrospinal fluid markers of AD and progression to clinical cognitive decline. **A**: CSF data were collected from patients via lumbar puncture. Both standard EEG and digital biomarkers were employed to classify CTR subjects and CSF + patients. **B**: Confusion matrices for the CTR/CSF + classification (digital biomarkers at the top and standard EEG biomarkers at the bottom). **C**: ROCs for the CTR/CSF + classification. **D**: Identification of CSF + patients with standard EEG biomarkers was non-conclusive (50% mean precision), while digital biomarkers achieved 87% precision. **E**: The machine-learning model pre-trained on the CTR/CSF + classification was used to classify between CSF- and CSF + patients (prediction of CSF positivity). **F**: Confusion matrices for the CSF-/CSF + classification (digital biomarkers at the top and standard EEG biomarkers at the bottom). **G**: ROCs for the CSF-/CSF + classification. **H**: The prediction of CSF positivity with standard EEG biomarkers was also non-conclusive (50% mean precision), while digital biomarkers achieved 81% precision. **I**: SCD patients underwent a 1-year follow-up to look for conversions to clinical cognitive decline. Both standard EEG and digital biomarkers were employed to classify stable and converted patients (prediction of clinical conversion). **J**: Confusion matrices for the stable/converted classification (digital biomarkers at the top and standard EEG biomarkers at the bottom). **K**: ROCs for the stable/converted classification. **L**: The prediction of converted patients with standard EEG biomarkers achieved limited results (4/7 correct predictions), while digital biomarkers predicted all (7/7) conversions. Significance notation: ** stands for $p < 0.01$, *** stands for $p < 0.001$. Error bars represent standard deviation values

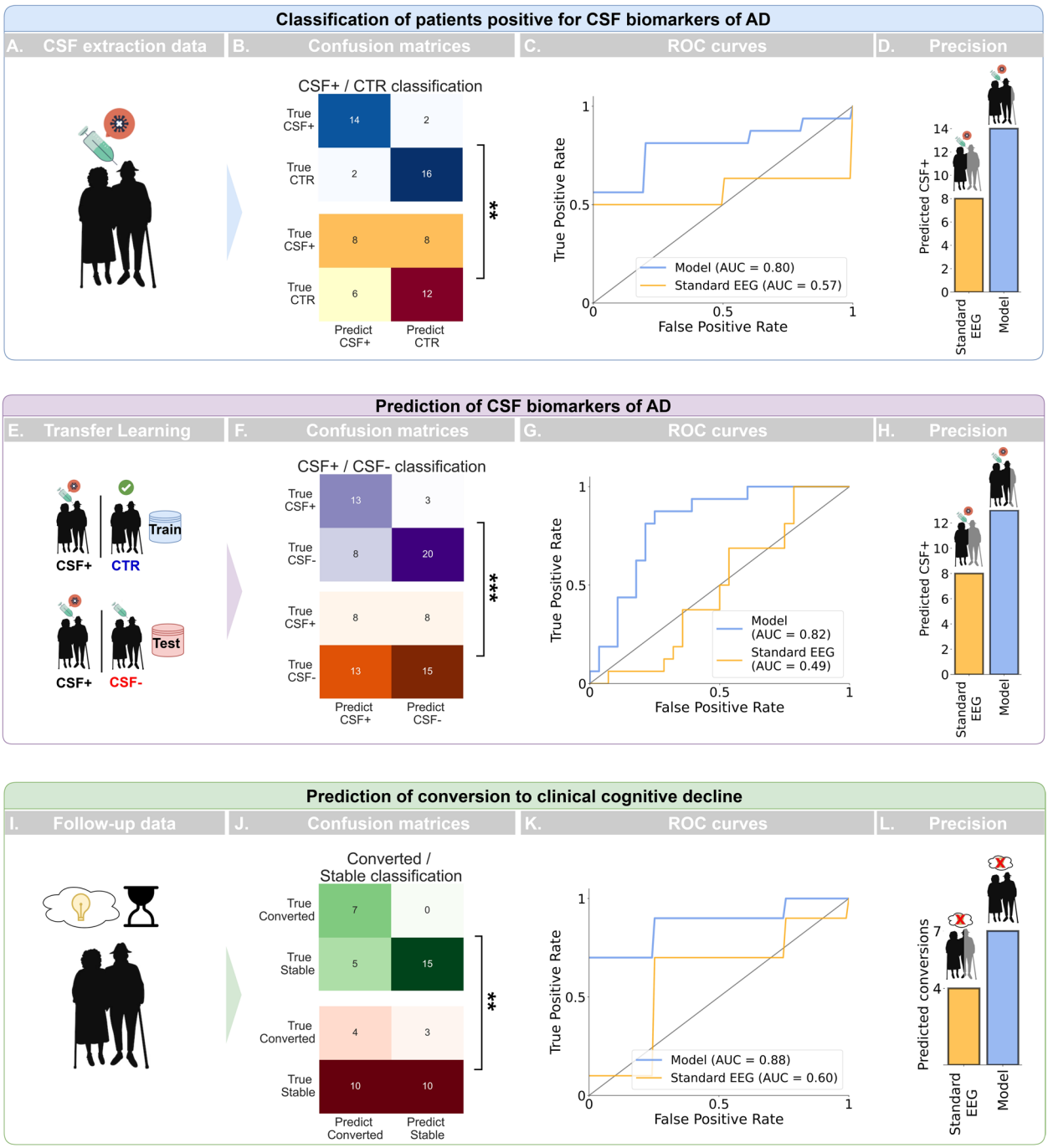


**Fig. 4** (See legend on previous page.)

Using a transfer learning approach, we assessed the ability of the classifier trained for the CSF +/CTR classification to support a prediction of CSF positivity for AD pathology by performing a classification of CSF + and CSF- patients (Fig. 4E). This procedure was repeated for both standard EEG and digital biomarkers. Strikingly, while the accuracy of standard EEG biomarkers was below chance level (accuracy 48% ± 7%, Fig. 4F bottom row), digital biomarkers achieved 76% ± 4% accuracy (top confusion matrix in Fig. 4F), Digital biomarkers also outperformed standard ones in terms of AUC (0.82 ± 0.07 vs 0.49 ± 0.06, see Fig. 4G) and precision (81% ± 3% vs 50% ± 4%, Fig. 4H). McNemar's test confirmed that the DADD-based classifier strongly outperformed

the one based on standard EEG biomarkers ($p = 0.0004$). Overall, digital biomarkers enabled highly accurate classification of CSF +/CTR participants and CSF +/CSF- patients, achieving a reliable prediction of CSF positivity in cognitive decline patients from EEG recordings.

Our study also comprised a one-year follow-up examination of cognitive status, which collected 27 SCD patients, 7 of whom converted to MCI. We first assessed the performance of standard EEG and digital biomarkers to discriminate between CTR subjects and converted patients. While no standard EEG biomarker was able to discriminate between conditions (N1 integral achieved best results with U = 38.0, $p = 0.25$, see Supplementary Fig. 4 A), the Connective Loss digital biomarker differed with high statistical significance between groups (Supplementary Fig. 4B, U = 114.0, $p = 0.0022$, d = 1.8).

We then attempted a machine-learning based prediction of early converters and stable SCD patients (Fig. 4I), comparing performances of standard EEG and digital biomarkers. Once again, digital biomarkers outperformed standard EEG in both accuracy (87% ± 8% vs 54% ± 7%, Fig. 4J) and AUC (0.88 ± 0.07 vs 0.60 ± 0.09, Fig. 4K). The differences between the two classifications were statistically significant (McNemar's test, $p = 0.008$). Notably, digital biomarkers successfully predicted all 7 conversions, while standard EEG biomarkers only identified 4/7 (Fig. 4L). These critical results demonstrate that biomarkers derived from digital twins can predict both CSF positivity and conversions to more severe conditions in patients in the AD continuum.

### Combining standard EEG and digital biomarkers led to optimal classification performance

Since both digital biomarkers and standard EEG features could differentiate between CTR subjects and SCD patients, we tested the performance of a machine learning model that combined both sets of features to classify patients and predict CSF positivity and clinical conversions. We selected the most informative feature from the two sets of biomarkers, one among standard EEG and one among digital biomarkers (respectively N1 integral and Connective Loss). This was done to enable comparisons with classifications based on standard EEG and digital biomarkers alone, for which we used two classifying features.

Combined features outperformed both standard EEG and digital biomarkers alone in classifying between SCD and CTR participants, (accuracy of 82% ± 3%, Fig. 5A). Combined biomarkers also significantly improved the AUC, which increased to 0.85 ± 0.03 (Fig. 5B). McNemar's test found relevant improvement over standard EEG biomarkers ($p = 0.002$), more pronounced than the differences between standard EEG biomarkers and digital biomarkers alone. This demonstrates a stronger classification capability when both feature types are combined, leading to a more accurate distinction between SCD patients and healthy subjects.

Similarly, we tested the performance of combined biomarkers in predicting converted SCD patients. Combined biomarkers improved the accuracy obtained using digital biomarkers (90% ± 4%, Fig. 5C), and they led to a substantial increase in AUC, reaching the value AUC = 0.98 ± 0.03 (Fig. 5D). McNemar's test confirmed highly significant differences between the classifications supported by combined biomarkers and the one based on standard EEG biomarkers only ($p = 0.004$). Combining standard and digital biomarkers did not improve the accuracy in the CSF +/CTR classification, nor in the CSF + prediction.

These results suggest that standard EEG and digital biomarkers provide complementary information about diagnostic categories. We validated this by performing a redundancy analysis, calculating pairwise mutual information between each biomarker (Supplementary Fig. 5). The analysis confirmed our hypothesis, revealing how the most informative EEG biomarkers (N1 integral and FC) had moderate to low redundancy with the most informative digital biomarkers (N1 integral: −0.13 MI with Neuroplasticity, −0.16 MI with Connective Loss; FC: −0.29 MI with Neuroplasticity, −0.27 MI with Connective Loss).

## Discussion

We utilized a personalized digital twin pipeline based on the DADD model and task-condition EEG recordings to derive robust biomarkers for Alzheimer's disease. Digital twins were reconstructed from EEG data through model inversion. We demonstrated that DADD model parameters are efficient digital biomarkers of Alzheimer's disease, even in its preclinical stages, accurately predicting both CSF positivity for AD biomarkers and conversions to clinical cognitive decline. All predictions were based on interpretable digital biomarkers that describe well-documented neurodegeneration mechanisms associated with AD [6, 29, 37–39], marking a significant leap forward in the progression toward early diagnosis.

We first tested the efficacy of digital biomarkers in classifying CTR subjects and SCD patients. Compared to standard biomarkers [15], digital biomarkers, particularly those related to structural connectivity [6, 48, 52], exhibited significant differences across CTR and SCD groups. Notably, the highly significant difference in Connective Loss values (Fig. 2I) between groups emphasizes the potential of our approach in identifying digital biomarkers that outperform standard ones in

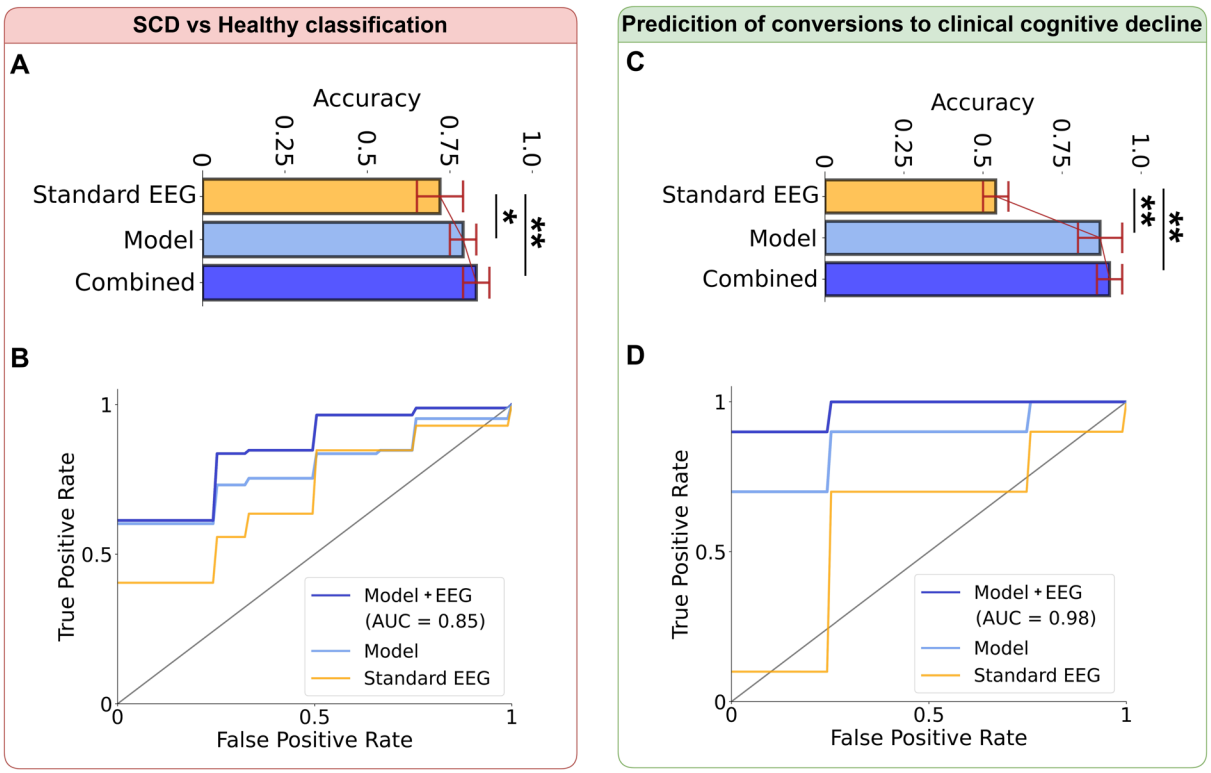


**Fig. 5** Combining standard EEG and digital biomarkers leads to optimal prediction of converted patients. **A**: Accuracy of SCD-CTR classification based on combined biomarkers was higher when compared to the accuracy of standard EEG and digital biomarkers alone. **B**: ROC curves for the SCD-CTR classifications reported in (A). The AUC was found to be higher when combining standard EEG and digital biomarkers. **C**: Accuracy of CSF + predictions based on standard EEG biomarkers, digital biomarkers or combined biomarkers. Accuracy was roughly equal when using digital biomarkers as classifying features or when combining digital with standard EEG biomarkers. **D**: ROC curves for CSF + classifications reported in (C). The AUC was higher for combined biomarkers. Significance notation: * stands for $p < 0.05$, ** stands for $p < 0.01$. Error bars represent standard deviation values

terms of discriminative power. It is worth mentioning that other studies based on computational modeling of AD introduced additional EEG metrics as candidate AD biomarkers, including viscous dynamics [53] and aperiodic component of the PSD [33]. While these approaches present promising alternatives, we focused on digital biomarkers derived from task-condition EEG metrics that allowed to characterize with good performance the evolution along the AD continuum [36, 44].

We tested the performance of digital biomarkers in classifying SCD and CTR participants, comparing results with a classification based on standard EEG biomarkers. The DADD-based classification achieved a mean accuracy of 79%, while the standard approach reached a lower accuracy of 72% (Fig. 3). Triebkorn et al. [34] also used a computational brain model to improve machine learning performance in classifying healthy individuals, MCI (mild cognitive impairment), and AD patients. Their results, however, focused on more advanced stages of the disease continuum and used digital biomarkers alongside standard features, boosting the f1-score from 0.64 to 0.74. In contrast, our preclinical classification reached a 79% accuracy using only model-derived digital biomarkers, increasing to 82% when standard EEG biomarkers were included.

Several previous studies have attempted to classify AD and cognitive decline patients using machine learning and non-invasive recordings. Fouladi et al. [22] reported a 92% accuracy in classifying healthy individuals and patients with overt symptoms of MCI and AD, employing a convolutional neural network and EEG recordings. Similarly, Sarraf and Tofighi [54] reached a 97% accuracy in classifying Alzheimer patients and healthy subjects by using a convolutional architecture trained on functional MRI data. All these studies dealt with more advanced stages of the disease, allowing for the classification of patients and healthy controls. In contrast, Sibilano et al. [21] reported a 0.76 f1-score in classifying SCD from MCI patients, and a 0.54 f1-score in the multiclass classification of healthy, SCD and MCI patients. These studies

rely heavily on deep neural network architectures, which, despite their accuracy, suffer from poor interpretability and require large datasets—often impractical in clinical settings where extensive data collection is challenging [21, 55]. On the contrary, we performed classifications based on only two features, with interpretable decision boundaries discriminating between different conditions.

Classifying patients as cognitive declined or healthy using biomarkers derived from non-invasive recordings is of limited clinical value, unless these biomarkers also predict key outcomes like CSF positivity for AD [10]. While several studies attempted an EEG-based classification of early Alzheimer stages, the prediction of CSF positivity based on non-invasive recordings has rarely been reported. Smailovic et al. [56] reported correlation between CSF markers and EEG metrics, but did not attempt a direct EEG-based prediction of CSF + patients. DADD instead enabled a high-precision identification of patients positive for CSF biomarkers of AD, achieving a mean accuracy of 88% and a precision of 87% (Fig. 4B-D). Additionally, when predicting CSF positivity among SCD and MCI patients, DADD achieved a mean accuracy of 76% with a mean precision of 81%, (Fig. 4F-H) demonstrating its potential in deriving robust biomarkers of Alzheimer's pathology from non-invasive recordings.

These results hold important clinical implications, as predicting CSF positivity from non-invasive recordings could greatly benefit patients and facilities by reducing the need for invasive and painful CSF extractions [57]. By combining the comfort and safety of EEG recordings with the diagnostic accuracy typically associated with CSF analysis, our approach represents a powerful tool for large-scale screening. This method could provide a diagnostic pathway for patients in prodromal AD phases like SCD, who are usually excluded from CSF extraction [58]. This exclusion is ubiquitous in developed areas, with studies showing that in some countries over 2/3 of clinics do not consider CSF extraction for diagnosing and characterizing the SCD condition [57]. By leveraging an affordable and widely available tool such as EEG, our approach also enhances the inclusivity of Alzheimer's diagnosis. Computational models and EEG recordings could provide a viable alternative to standard brain imaging methods such as MRI [59] and PET [60], that require far more expensive machinery, which would limit the access to Alzheimer's diagnosis in several developing areas [61, 62].

One of the key challenges of dementia research is to forecast future conversions using widely available diagnostic tools [4]. Our findings also demonstrate that digital biomarkers derived from our computational approach successfully predicted all conversions (7/7) from SCD to clinical cognitive decline a full year in advance (Fig. 4J-L). The classification between (early) converters and stable patients achieved 87% accuracy. Standard EEG biomarkers, in contrast, performed significantly worse (54% mean accuracy), reinforcing the superior predictive power of DADD. Engedal et al. [63] have reported a 69% accuracy in predicting conversion from quantitative EEG analysis. Westman et al. [64] reported an accuracy of 83% in predicting MCI converted to AD after 1-year follow-up with combined CSF and MRI data. DADD led to similar accuracy levels, but in patients in preclinical stages of the disease. Furthermore, DADD- based prediction was achieved leveraging only EEG data combined with a digital twin approach, highlighting the potential of digital biomarkers as early predictors of pathological cognitive decline. An advancement in early detection using affordable and non-invasive methods has significant implications for timely intervention and personalized treatment strategies, offering the potential to improve patient outcomes, slowing the progression of Alzheimer's disease and drastically reducing clinical expenses [4]. Furthermore, while digital biomarkers independently offered superior prognostic performance compared to standard EEG biomarkers in predicting conversions, combining the two further enhanced prediction accuracy. This suggests that digital twins provide complementary information to metrics obtainable from standard EEG analysis, supporting their combined use for optimal prognostic performance.

It is worth noting that the study presents several limitations. First, the sample sizes used for ERP analysis are uneven, notably the numerosity of the CTR group is smaller than that of the SCD one. The total numerosity of the dataset is also small, and results need to be generalized to larger cohorts. Furthermore, the numerosity of CSF + and converted patients was even smaller, limiting the generalizability and statistical power of our findings. Another potential issue is the use of the same dataset for the determination of decision boundaries in patients' classification and for the prediction of CSF positivity and clinical conversion. This could induce overfitting, further reducing generalizability and inflating performances. This limitation was addressed by adopting a nested cross validation approach to reduce overfitting (see Supplementary Materials). To further address these limitations, we are conducting an ongoing study, applying the DADD model to a much larger dataset, also encompassing a larger time window for follow-up examination. To ensure generalizability, we are also conducting a multicentric study, in which the model is employed with a transfer learning approach to derive decision boundaries for patients' diagnosis across different centers adopting different recording modalities. This will ensure the cross-applicability of the DADD model to different cohorts

presenting different numerosity, recording techniques, pre-processing methodologies and inclusion criteria. Furthermore, the study primarily focuses on ERP neural markers and FC. Given that cognitive decline is a multifaced condition characterized by complex mechanisms it is crucial to investigate other relevant aspects of its progression. Lastly, although the DADD model is capable of reconstructing structural alterations underpinning preclinical AD, it is still a simplified representation of the complex biological processes involved in the disease continuum. Future iterations of the model should enhance biological realism and consider additional factors that contribute to cognitive decline and anomalies in neural activity during cognitive task execution. Further research should also aim to better understand the degeneration mechanisms driving cognitive decline and their clinical implications, ultimately leading to improved diagnostic and therapeutic strategies.

## Conclusion

The integration of the DADD model in the assessment of Alzheimer's progression presents a significant advancement over current methods. Digital biomarkers offer an interpretable, efficient, and cost-effective alternative to standard biomarkers, providing significant benefits in the early identification of the condition. Our approach aligns with the growing emphasis on precision medicine and digital biomarkers, presenting an accurate and interpretable tool for early AD diagnosis. Since our digital biomarkers are sensitive to early stages of cognitive decline—such as Subjective Cognitive Decline—they hold strong potential for early AD detection. Specifically, they could be integrated into software tools that complement routine EEG analysis in clinical settings, flagging subtle neurophysiological changes that may precede overt symptoms. Beyond initial screening, these biomarkers could also be applied in longitudinal EEG monitoring, offering a non-invasive and cost-effective way to track the evolution of neurodegeneration over time along the cognitive decline continuum. This could potentially take place in combination with emerging techniques for AD diagnosis such as plasma biomarkers [65]. Moreover, when combined with structural imaging methods like MRI or PET, our framework could enable the construction of highly personalized trajectories of disease progression by linking functional impairments to underlying multiscale structural changes. This multimodal integration could enhance both diagnostic precision and individualized planning for intervention or follow-up.

## Supplementary Information

The online version contains supplementary material available at https://doi.org/10.1186/s13195-025-01765-z.

Supplementary Material 1.

**Authors' contributions**

LGA and AM conceived the data analysis and the simulations. LGA performed the simulations. LGA, AAV, ML and JC performed the data analysis. AM supervised data analysis and simulations. LGA and AM wrote the first draft of the manuscript. AG, VB and SS conceived and supervised data collection. VB, RB, SM, GG, GG, FE, MS, CF, GS, provided clinical care and performed data acquisition, VM, CM, SP, BN performed data acquisition. All authors critically revised the manuscript.

**Funding**

This project is funded by Tuscany Region—PRedicting the EVolution of SubjectIvE Cognitive Decline to Alzheimer's Disease With machine learning – PREVIEW CUP.D18D20001300002.
THE ("Tuscany Health Ecosystem") Project funded by the Italian Ministry of University and Research—PNRR—Next Generation EU Projects Project funded under the National Recovery and Resilience Plan (NRRP), Mission 4 Component 2 Investment 1.3—Call for tender No. 341 of 15/03/2022 of Italian Ministry of University and Research funded by the European Union – NextGenerationEU Award Number: Project code PE0000006, Concession Decree No. 1553 of 11/10/2022 adopted by the Italian Ministry of University and Research, CUP D93 C22000930002, "A multiscale integrated approach to the study of the nervous system in health and disease" (MNESYS).

**Data availability**

Patient data can be provided pending scientific review and a completed material transfer agreement. Requests for patient data should be submitted to the corresponding author: alberto.mazzoni@santannapisa.it. Code for the DADD model can be found in https://github.com/LoreAma/Code_AD_simulations/. Code for model inversion and machine learning pipeline can be provided upon request to LorenzoGaetano.Amato@santannapisa.it.

## Declarations

**Ethics approval and consent to participate**

Participant recruitment and EEG recordings adhered to the guidelines set forth by the Declaration of Helsinki and the standards outlined by the Committee on Human Experimentation of the Careggi University Hospital in Florence, Italy. The study received approval from the local Institutional Review Board ("Comitato Etico di Area Vasta Centro", reference 15691oss). All participants gave informed consent before being enrolled in this study.

**Competing interests**

The authors declare no competing interests.

**Author details**

[1]The BioRobotics Institute, Sant'Anna School of Advanced Studies, Piazza Martiri Della Libertà 33, 56127 Pisa, Italy. [2]Department of Excellence in Robotics and AI, Sant'Anna School of Advanced Studies, Piazza Martiri della Libertà 33, 56127 Pisa, Italy. [3]Research and Innovation Center for Dementia-CRIDEM, Careggi University Hospital, Largo Brambilla 3, 50134 Florence, Italy. [4]Vita-Salute San Raffaele University, Via Olgettina 60, 20132 Milan, Italy. [5]IRCCS Policlinico San Donato, Edmondo Malan 2, 20097 Milan, Italy. [6]Skeletal Muscles and Sensory Organs Department, Careggi University Hospital, Largo Brambilla 3, 50134 Florence, Italy. [7]IRCSS Fondazione Don Carlo Gnocchi, Via Di Scandicci 269, 50143 Florence, Italy. [8]Unit of Neurophysiology, Careggi University Hospital, Florence, Italy. [9]Department of Neuroscience, Psychology, Drug Research and Child Health, Università Di Firenze, Largo Brambilla 3, 50134 Florence, Italy.

Received: 11 February 2025 Accepted: 13 May 2025
Published online: 31 May 2025

**References**


1. Prince M, Wimo A, Guerchet M, Ali GC, Wu YT, Prina M. World Alzheimer Report 2015. The Global Impact of Dementia: An analysis of prevalence, incidence, cost and trends. 2015. https://www.alzint.org/u/WorldAlzheimerReport2015.pdf.
2. International AD. World Alzheimer Report 2023: Reducing Dementia Risk: Never too early, never too late. Published online September 21, 2023. Accessed February 16, 2024. https://www.alzint.org/resource/world-alzheimer-report-2023/
3. Nandi A, Counts N, Chen S, et al. Global and regional projections of the economic burden of Alzheimer's disease and related dementias from 2019 to 2050: A value of statistical life approach. eClinicalMedicine. 2022;51. https://doi.org/10.1016/j.eclinm.2022.101580
4. Rasmussen J, Langerman H. Alzheimer's disease – why we need early diagnosis. Degener Neurol Neuromuscul Dis. 2019;9:123–30. https://doi.org/10.2147/DNND.S228939.
5. Jessen F, Amariglio RE, Buckley RF, et al. The characterisation of subjective cognitive decline. Lancet Neurol. 2020;19(3):271–8. https://doi.org/10.1016/S1474-4422(19)30368-0.
6. Ohlhauser L, Parker AF, Smart CM, Gawryluk JR. White matter and its relationship with cognition in subjective cognitive decline. Alzheimers Dement Diagn Assess Dis Monit. 2019;11:28–35. https://doi.org/10.1016/j.dadm.2018.10.008.
7. Arrondo P, Elía-Zudaire Ó, Martí-Andrés G, Fernández-Seara MA, Riverol M. Grey matter changes on brain MRI in subjective cognitive decline: a systematic review. Alzheimers Res Ther. 2022;14(1):98. https://doi.org/10.1186/s13195-022-01031-6.
8. Fogel H, Levy-Lamdan O, Zifman N, et al. Brain network integrity changes in subjective cognitive decline: a possible physiological biomarker of dementia. Front Neurol. 2021;12:699014.
9. Ossenkoppele R, Jagust WJ. The complexity of subjective cognitive decline. JAMA Neurol. 2017;74(12):1400–2. https://doi.org/10.1001/jamaneurol.2017.2224.
10. Ulbl J, Rakusa M. The importance of subjective cognitive decline recognition and the potential of molecular and neurophysiological biomarkers—a systematic review. Int J Mol Sci. 2023;24(12):10158. https://doi.org/10.3390/ijms241210158.
11. Vesikansa A, Halminen O, Mehtälä J, et al. Early start of anti-dementia medication is associated with lower health and social care costs in Alzheimer´s patients: a Finnish nationwide register study. Eur J Health Econ. 2023;24(9):1421–8. https://doi.org/10.1007/s10198-022-01553-8.
12. Getsios D, Blume S, Ishak KJ, Maclaine G, Hernández L. An economic evaluation of early assessment for Alzheimer's disease in the United Kingdom. Alzheimers Dement. 2012;8(1):22–30. https://doi.org/10.1016/j.jalz.2010.07.001.
13. Bahar-Fuchs A, Clare L, Woods B. Cognitive training and cognitive rehabilitation for mild to moderate Alzheimer's disease and vascular dementia - Bahar-Fuchs, A - 2013 | Cochrane Library. Accessed August 16, 2024. https://www.cochranelibrary.com/cdsr/doi/https://doi.org/10.1002/14651858.CD003260.pub2/full
14. Jackson AF, Bolger DJ. The neurophysiological bases of EEG and EEG measurement: a review for the rest of us. Psychophysiology. 2014;51(11):1061–71. https://doi.org/10.1111/psyp.12283.
15. Horvath A, Szucs A, Csukly G, Sakovics A, Stefanics G, Kamondi A. EEG and ERP biomarkers of Alzheimer's disease: a critical review. Front Biosci Landmark Ed. 2018;23:183–220.
16. Meghdadi AH, Karić MS, McConnell M, et al. Resting state EEG biomarkers of cognitive decline associated with Alzheimer's disease and mild cognitive impairment. PLoS ONE. 2021;16(2):e0244180. https://doi.org/10.1371/journal.pone.0244180.
17. Meghdadi AH, Salat D, Hamilton J, et al. EEG and ERP biosignatures of mild cognitive impairment for longitudinal monitoring of early cognitive decline in Alzheimer's disease. PLoS ONE. 2024;19(8):e0308137. https://doi.org/10.1371/journal.pone.0308137.
18. Farina FR, Emek-Savaş DD, Rueda-Delgado L, et al. A comparison of resting state EEG and structural MRI for classifying Alzheimer's disease and mild cognitive impairment. Neuroimage. 2020;215:116795. https://doi.org/10.1016/j.neuroimage.2020.116795.
19. Ferree TC, Clay MT, Tucker DM. The spatial resolution of scalp EEG. Neurocomputing. 2001;38–40:1209–16. https://doi.org/10.1016/S0925-2312(01)00568-9.
20. van den Broek SP, Reinders F, Donderwinkel M, Peters M. Volume conduction effects in EEG and MEG. Electroencephalogr Clin Neurophysiol. 1998;106(6):522–34.
21. Sibilano E, Brunetti A, Buongiorno D, et al. An attention-based deep learning approach for the classification of subjective cognitive decline and mild cognitive impairment using resting-state EEG. J Neural Eng. 2023;20(1):016048.
22. Fouladi S, Safaei AA, Mammone N, Ghaderi F, Ebadi MJ. Efficient deep neural networks for classification of Alzheimer's disease and mild cognitive impairment from scalp EEG recordings. Cogn Comput. 2022;14(4):1247–68. https://doi.org/10.1007/s12559-022-10033-3.
23. Hata M, Watanabe Y, Tanaka T, et al. Precise discrimination for multiple etiologies of dementia cases based on deep learning with electroencephalography. Neuropsychobiology. 2023;82(2):81–90. https://doi.org/10.1159/000528439.
24. Morabito FC, Campolo M, Ieracitano C, et al. Deep convolutional neural networks for classification of mild cognitive impaired and Alzheimer's disease patients from scalp EEG recordings. In: 2016 IEEE 2nd International Forum on Research and Technologies for Society and Industry Leveraging a Better Tomorrow (RTSI). ; 2016:1–6. https://doi.org/10.1109/RTSI.2016.7740576
25. Kim NH, Yang DW, Choi SH, Kang SW. Machine Learning to Predict Brain Amyloid Pathology in Pre-dementia Alzheimer's Disease Using QEEG Features and Genetic Algorithm Heuristic. Front Comput Neurosci. 2021;15. https://doi.org/10.3389/fncom.2021.755499
26. Qiu S, Joshi PS, Miller MI, et al. Development and validation of an interpretable deep learning framework for Alzheimer's disease classification. Brain. 2020;143(6):1920–33. https://doi.org/10.1093/brain/awaa137.
27. Qiu S, Miller MI, Joshi PS, et al. Multimodal deep learning for Alzheimer's disease dementia assessment. Nat Commun. 2022;13(1):3404. https://doi.org/10.1038/s41467-022-31037-5.
28. Glomb K, Cabral J, Cattani A, Mazzoni A, Raj A, Franceschiello B. Computational Models in Electroencephalography. Brain Topogr. 2022;35(1):142–61. https://doi.org/10.1007/s10548-021-00828-2.
29. Stefanovski L, Meier JM, Pai RK, et al. Bridging scales in Alzheimer's disease: biological framework for brain simulation with the virtual brain. Front Neuroinformatics. 2021;15:630172. https://doi.org/10.3389/fninf.2021.630172.
30. Stefanovski L, Triebkorn P, Spiegler A, et al. Linking molecular pathways and large-scale computational modeling to assess candidate disease mechanisms and pharmacodynamics in Alzheimer's disease. Front Comput Neurosci. 2019;13:54. https://doi.org/10.3389/fncom.2019.00054.
31. Van Nifterick AM, Gouw AA, Van Kesteren RE, Scheltens P, Stam CJ, De Haan W. A multiscale brain network model links Alzheimer's disease-mediated neuronal hyperactivity to large-scale oscillatory slowing. Alzheimers Res Ther. 2022;14(1):101. https://doi.org/10.1186/s13195-022-01041-4.
32. Cabrera-Álvarez J, Stefanovski L, Martin L, Susi G, Maestú F, Ritter P. A Multiscale closed-loop neurotoxicity model of Alzheimer's disease progression explains functional connectivity alterations. eNeuro. 2024;11(4). https://doi.org/10.1523/ENEURO.0345-23.2023
33. Martínez-Cañada P, Perez-Valero E, Minguillon J, Pelayo F, López-Gordo MA, Morillas C. Combining aperiodic 1/f slopes and brain simulation: An EEG/MEG proxy marker of excitation/inhibition imbalance in Alzheimer's disease. Alzheimers Dement Diagn Assess Dis Monit. 2023;15(3):e12477. https://doi.org/10.1002/dad2.12477.
34. Triebkorn P, Stefanovski L, Dhindsa K, et al. Brain simulation augments machine-learning–based classification of dementia. Alzheimers Dement Transl Res Clin Interv. 2022;8(1): e12303. https://doi.org/10.1002/trc2.12303.
35. Amato LG, Vergani AA, Lassi M, et al. Personalized modeling of Alzheimer's disease progression estimates neurodegeneration severity from EEG recordings. Alzheimers Dement Diagn Assess Dis Monit. 2024;16(1):e12526. https://doi.org/10.1002/dad2.12526.
36. Amato LG, Vergani AA, Lassi M, et al. Personalized brain models link cognitive decline progression to underlying synaptic and connectivity degeneration. Alzheimers Res Ther. 2025;17(1):74. https://doi.org/10.1186/s13195-025-01718-6.
37. Phillips DJ, McGlaughlin A, Ruth D, Jager LR, Soldan A. Graph theoretic analysis of structural connectivity across the spectrum of Alzheimer's

disease: The importance of graph creation methods. NeuroImage Clin. 2015;7:377–90. https://doi.org/10.1016/j.nicl.2015.01.007.
38. Vance DE, Roberson AJ, McGuinness TM, Fazeli PL. How neuroplasticity and cognitive reserve: protect cognitive functioning. J Psychosoc Nurs Ment Health Serv. 2010;48(4):23–30. https://doi.org/10.3928/02793695-20100302-01.
39. Ren SQ, Yao W, Yan JZ, et al. Amyloid β causes excitation/inhibition imbalance through dopamine receptor 1-dependent disruption of fast-spiking GABAergic input in anterior cingulate cortex. Sci Rep. 2018;8(1):302.
40. Mazzeo S, Lassi M, Padiglioni S, et al. PRedicting the EVolution of SubjectIvE cognitive decline to Alzheimer's disease with machine learning: the PREVIEW study protocol. BMC Neurol. 2023;23(1):300. https://doi.org/10.1186/s12883-023-03347-8.
41. Albert MS, DeKosky ST, Dickson D, et al. The diagnosis of mild cognitive impairment due to Alzheimer's disease: recommendations from the National Institute on Aging-Alzheimer's Association workgroups on diagnostic guidelines for Alzheimer's disease. Alzheimers Dement. 2011;7(3):270–9.
42. Delorme A, Makeig S. EEGLAB: an open source toolbox for analysis of single-trial EEG dynamics including independent component analysis. J Neurosci Methods. 2004;134(1):9–21.
43. Bigdely-Shamlo N, Mullen T, Kothe C, Su KM, Robbins KA. The PREP pipeline: standardized preprocessing for large-scale EEG analysis. Front Neuroinform. 2015;9:16.
44. Vergani AA, Mazzeo S, Moschini V, et al. Event-related potential markers of subjective cognitive decline and mild cognitive impairment during a sustained visuo-attentive task. NeuroImage Clin. 2025;45:103760. https://doi.org/10.1016/j.nicl.2025.103760.
45. Hansson O, Batrla R, Brix B, et al. The Alzheimer's Association international guidelines for handling of cerebrospinal fluid for routine clinical measurements of amyloid β and tau. Alzheimers Dement J Alzheimers Assoc. 2021;17(9):1575–82. https://doi.org/10.1002/alz.12316.
46. Sanz Leon P, Knock SA, Woodman MM, et al. The virtual brain: a simulator of primate brain network dynamics. Front Neuroinform. 2013;7:10.
47. Jansen BH, Rit VG. Electroencephalogram and visual evoked potential generation in a mathematical model of coupled cortical columns. Biol Cybern. 1995;73(4):357–66. https://doi.org/10.1007/BF00199471. PMID: 7578475.
48. Stam CJ. Hub overload and failure as a final common pathway in neurological brain network disorders. Netw Neurosci. 2024;8(1):1–23. https://doi.org/10.1162/netn_a_00339.
49. Sanz-Leon P, Knock SA, Spiegler A, Jirsa VK. Mathematical framework for large-scale brain network modeling in the virtual brain. Neuroimage. 2015;111:385–430.
50. Braak H, Braak E. Neuropathological stageing of Alzheimer-related changes. Acta Neuropathol (Berl). 1991;82(4):239–59.
51. Bastos AM, Schoffelen JM. A Tutorial Review of Functional Connectivity Analysis Methods and Their Interpretational Pitfalls. Front Syst Neurosci. 2016;9. https://doi.org/10.3389/fnsys.2015.00175
52. Vernooij MW, de Groot M, van der Lugt A, et al. White matter atrophy and lesion formation explain the loss of structural integrity of white matter in aging. Neuroimage. 2008;43(3):470–7. https://doi.org/10.1016/j.neuroimage.2008.07.052.
53. Coronel-Oliveros C, Gómez RG, Ranasinghe K, et al. Viscous dynamics associated with hypoexcitation and structural disintegration in neurodegeneration via generative whole-brain modeling. Alzheimers Dement. 2024;20(5):3228–50. https://doi.org/10.1002/alz.13788.
54. Sarraf S, Tofighi G. Classification of Alzheimer's Disease using fMRI Data and Deep Learning Convolutional Neural Networks. Published online March 29, 2016. https://doi.org/10.48550/arXiv.1603.08631
55. Hu X, Chu L, Pei J, Liu W, Bian J. Model complexity of deep learning: a survey. Knowl Inf Syst. 2021;63(10):2585–619. https://doi.org/10.1007/s10115-021-01605-0.
56. Smailovic U, Koenig T, Kåreholt I, et al. Quantitative EEG power and synchronization correlate with Alzheimer's disease CSF biomarkers. Neurobiol Aging. 2018;63:88–95. https://doi.org/10.1016/j.neurobiolaging.2017.11.005.
57. Bartels C, Kögel A, Schweda M, et al. Use of cerebrospinal fluid biomarkers of Alzheimer's disease risk in mild cognitive impairment and subjective cognitive decline in routine clinical care in Germany. J Alzheimers Dis. 2020;78(3):1137–48. https://doi.org/10.3233/JAD-200794.
58. Duits FH, Martinez-Lage P, Paquet C, et al. Performance and complications of lumbar puncture in memory clinics: Results of the multicenter lumbar puncture feasibility study. Alzheimers Dement. 2016;12(2):154–63. https://doi.org/10.1016/j.jalz.2015.08.003.
59. McMahon PM, Araki SS, Neumann PJ, Harris GJ, Gazelle GS. Cost-effectiveness of functional imaging tests in the diagnosis of Alzheimer disease. Radiology. 2000;217(1):58–68. https://doi.org/10.1148/radiology.217.1.r00se1358.
60. McMahon PM, Araki SS, Sandberg EA, Neumann PJ, Gazelle GS. Cost-effectiveness of PET in the diagnosis of Alzheimer disease. Radiology. 2003;228(2):515–22. https://doi.org/10.1148/radiol.2282020915.
61. Jalloul M, Miranda-Schaeubinger M, Noor AM, et al. MRI scarcity in low- and middle-income countries. NMR Biomed. 2023;36(12):e5022. https://doi.org/10.1002/nbm.5022.
62. Gallach M, Lette MM, Abdel-Wahab M, Giammarile F, Pellet O, Paez D. Addressing Global Inequities in Positron Emission Tomography-Computed Tomography (PET-CT) for Cancer Management: A Statistical Model to Guide Strategic Planning. Med Sci Monit. 2020;26:0–0. https://doi.org/10.12659/MSM.926544
63. Engedal K, Barca ML, Høgh P, et al. The power of EEG to predict conversion from mild cognitive impairment and subjective cognitive decline to dementia. Dement Geriatr Cogn Disord. 2020;49(1):38–47. https://doi.org/10.1159/000508392.
64. Westman E, Muehlboeck JS, Simmons A. Combining MRI and CSF measures for classification of Alzheimer's disease and prediction of mild cognitive impairment conversion. Neuroimage. 2012;62(1):229–38. https://doi.org/10.1016/j.neuroimage.2012.04.056.
65. Blennow K, Galasko D, Perneczky R, et al. The potential clinical value of plasma biomarkers in Alzheimer's disease. Alzheimers Dement. 2023;19(12):5805–16. https://doi.org/10.1002/alz.13455.

## Publisher's Note